

A model of interaction of Phobos' surface with the martian environment

F. Cipriani^a, O. Witasse^{a,*}, F. Leblanc^b, R. Modolo^b, R.E. Johnson^c

^a ESA/ESTEC, Research and Scientific Support Department, Keplerlaan 1, PO Box 299, Noordwijk, 2200 AG, The Netherlands

^b LATMOS, 11 Boulevard D'Alembert, 78280 Guyancourt, France

^c Department of Materials Science & Engineering, University of Virginia, Charlottesville, VA 22904, United States

ARTICLE INFO

Article history:

Received 8 July 2010

Revised 27 January 2011

Accepted 31 January 2011

Keywords:

Mars

Solar wind

Moon

ABSTRACT

We simulate space weathering of Phobos' surface due to both sputtering by solar wind ions (H^+ and He^{2+}) and planetary protons, and surface material vaporization by micrometeoroids impact. Assuming an Iron-rich composition of Phobos' regolith, we find that densities of neutral species (Fe, O, Al, Ca, Mg, Na) in the martian environment are in the range (10^{-4} – 10^{-1} cm^{-3}), and observe an ejecta disk with a radius of 6 martian radii in the equatorial plane and a thickness of 3 martian radii in the perpendicular plane. In order to determine the observability of such species from space based instruments, we also estimate their solar scattering emission line intensities. We conclude that Magnesium would be the only potential candidate suitable for spectral detection.

© 2011 Elsevier Inc. All rights reserved.

1. Introduction

Phobos is a non spherical body (mean radius 11 km) with a quasi-circular and equatorial orbit located only 9377 km from Mars centre. Phobos' orbital period is only 7.65 h, about 30% of a Mars day. The existence of gas/dust tori at Phobos and Deimos orbits has been previously postulated (Soter, 1971; Ip and Banaszekiewicz, 1990). However Earth based optical observations have failed to detect their signatures. Recent observations from Hubble Space Telescope fix an optical depth limit for Phobos dust ring of 10^{-8} in a wavelength range 440–740 nm (Showalter et al., 2006). Moreover, the presence of ring structures has recently been ruled out (Øieroset et al., 2010) as the cause of the plasma perturbations events detected during the Phobos-2 mission (Dubinin et al., 1990) close to Phobos orbit. The density of such structures, if they exist, is therefore very low. In the present paper we use a 3D Monte Carlo model to simulate sputtering of Phobos surface by solar wind ions and material vaporization due to micrometeoroid bombardment in the martian environment. We derive densities (covering a range $\sim 10^{-4}$ – 10^{-1} cm^{-3}) of neutral species assumed to be in Phobos' regolith as Fe, O, Mg, Al, Ca, Na, outgassed in the martian environment, and study the morphology of the ejecta cloud. In order to infer observability of the neutral cloud from ground or space based instruments, we give estimates of solar scattering emission brightness for each species.

2. Monte Carlo model

We carried out a 3D Monte Carlo numerical simulation of neutral species ejected from Phobos' surface. Our model has been

derived from that recently used at Europa (Leblanc et al., 2005; Cipriani et al., 2008, 2009). In this model trajectories of neutral particles are followed in a gravitational system formed by Mars, Phobos and Deimos. Particles are also subject to the solar radiation pressure determined for an average Mars–Sun distance and using photon fluxes at Doppler shifted absorption lines of Fe, O, Mg, Al, Ca, Na. Simulations are carried out at solar minimum conditions. We consider that Phobos' surface is mainly subject to sputtering by solar wind ions or planetary ions, and micrometeoroid bombardment. Therefore other sources of ejection, such as impact of atoms from the hot corona or dusts rings/ejecta particles (i.e., self sustaining ring), as well as thermal outgassing, are neglected. Neutral particles are lost when they impact Mars surface, or escape the martian gravitational field, or become ionized either by solar photons or in charge exchange reactions with solar wind protons. From assumptions on the surface composition given in Section 2.1, the neutral species considered are Na, Ca, Al, Fe, O and Mg. We use charge exchange cross sections with H^+ from Kuback and Sidis (1981) for Na, Rutherford and Vroom (1972) for Fe, Pandey et al. (2007) for Ca, Mg and Al, Stebbings et al. (1964) for O. For all species we assume slow variations of the cross sections around 1 keV, the average energy of the solar wind protons distribution. That is, charge exchange reaction cross sections do not depend on particle energy in our simulation. Photoionization rates at Mars' distance are derived from Huebner et al. (1992), Fulle et al. (2007), and Molina-Cuberos et al. (2003).

2.1. Surface composition

A good agreement is observed between Phobos IR surface spectra and spectra of D-types asteroids (see for instance Rivkin et al.

* Corresponding author.

E-mail address: owitasse@rssd.esa.int (O. Witasse).

(2002). From composition of analog Iron-rich meteorites (Vernazza et al., 2010), we assume a putative Iron-rich composition of Phobos' surface regolith (see Table 1). This is also consistent with a large reddening of the IR spectra due to preferential removal of Oxygen leaving Iron in a reduced state during the weathering process (e.g. Johnson and Baragiola, 1991; Hapke, 2001). Since Phobos' near surface bulk density is close to 1.8 g cm^{-3} (Jacobson, 2008), and reasonably close to Mercury's regolith bulk density (Cintala, 1992), we derive estimates of surface concentration of species from comparison of mass fraction of elements assumed to be present on both (as Sodium).

2.2. Sputtering

Phobos' surface is subject to weathering by protons and alpha particles from the solar wind. At solar minimum the average flux at Mars's orbit is close to $9 \times 10^7 \text{ cm}^{-2} \text{ s}^{-1}$, with 5% of the flux being He^{2+} ions. He^{2+} ions significantly contribute to the sputtering process (Johnson and Baragiola, 1991). The ratio of (momentum transfer) sputtering yields for H^+ and He^{2+} ions is close to ~ 0.1 , and is taken into account in our simulation. Sputtering yields of oxidized Iron have been derived by Behrisch (1980). In the present work we assume such yields can be taken as proxy for sputtering of Phobos' surface, and use a yield of 0.06/ion, accounting for Phobos' high porosity (possibly much larger than 40% after Busch et al. (2007)). This yield value is very similar to the yield used by Leblanc and Johnson (2003) at Mercury (though consistent with a silicate dominated matrix). We assume that no change of stoichiometry occurs in the regolith due to sputtering, that is, composition does not change within the timescale of the simulation. In practice, since Fe and O are the main sputtered species (sputtered atoms essentially escape Phobos's very low gravity field), yields of other species are scaled to Iron by multiplying the Iron yield by their surface concentration. Plasma conditions at Phobos orbit (ions densities and velocities) are computed from outputs of a Hybrid simulation of the solar wind interaction with Mars (Modolo et al., 2005) carried out at solar minimum conditions. Since all ejected particles basically escape Phobos' field, simulation results are not very sensitive to the energy distributions of ejecta. Therefore, we use energy distributions scaled to that of Sodium sputtered from Mercury's regolith as given in Leblanc and Johnson (2003), except for Iron and Oxygen for which we use the distributions measured by Matsuda et al. (1988).

2.3. Micro-meteoritic bombardment

The flux of meteoroids at Mars (in the mass range $10^{-3}/10 \text{ g}$) represents about half the flux at the Earth (Christou and Beurle, 1999). An estimate of 10^{-6} meteoroids $\text{km}^{-2} \text{ h}^{-1}$ can be derived from Domokos et al. (2007) and Molina-Cuberos et al. (2003). The number S_a (in $\text{cm}^{-2} \text{ s}^{-1}$) of atoms of species a vaporized during an impact is given by (see for instance Bruno et al. (2007)) $S_a = M_{vap} * (f_a/m_a) * N_A$ where M_{vap} is the flux of vaporized material ($\text{g cm}^{-2} \text{ s}^{-1}$), f_a is the mass fraction of a in the regolith, m_a is the atomic mass, and N_A the Avogadro number. M_{vap} can be computed from a number of assumptions on surface and impactors properties as regolith density, size and velocity distributions of impactors, and impact pressure (e.g. Killen et al., 2001), to which large uncertainties are associated. However in the present study, based on

Table 1
Mass fraction of the main elements composing Phobos' regolith, used in this study.

Element	Fe	Si	O	Mg	Al	Na	Ca
Mass fraction	0.21	0.1300	0.4100	0.10	0.017	0.005	0.001

vaporized fluxes estimates at Mercury ($5 \times 10^{-15} \text{ g cm}^{-2} \text{ s}^{-1}$) and the Moon ($7 \times 10^{-17} \text{ g cm}^{-2} \text{ s}^{-1}$) (Cintala, 1992, Bruno et al., 2007) we assume a vaporized flux of $6 \times 10^{-19} \text{ g cm}^{-2} \text{ s}^{-1}$ for present calculations at Mars orbit. Due to the small size of Phobos we assume a uniform flux at Phobos' surface. Corresponding ejection rates per species are given in Table 2. We follow the same approach as in Leblanc and Johnson (2003) who modelled ejection of Sodium atoms due to impact vaporization of Mercury's regolith. Here we also use an Maxwellian energy distribution of ejected particles with a temperature of 3000 K, in good agreement with the temperature of vapour produced by hypervelocity particle impacts on solid target reported in Eichhorn (1978).

3. Simulation results

The phase angle α used in the text and figures to define Phobos' orbital position is drawn in Fig. 1 over a distribution of the magnetic field intensity in Mars' equatorial plane (X - Y) derived by Modolo et al. (2005) with an angle between the solar wind velocity vector and Interplanetary Magnetic Field of 56° . The X axis is along the Sun–Mars direction. The phase angle origin is when Phobos is on the dusk side of Mars.

3.1. Ejecta densities and neutral cloud morphology

Variations of average ejecta densities within 500 km from Phobos surface are shown for each species in the lower panel of Fig. 2 as a function of Phobos phase angle, while the middle and upper panels respectively showing variations of the protons velocity component collinear to the Mars–Sun axis (blue line), and the solar wind proton density at Phobos' orbit (red line). The evolution of the degassing is clearly correlated with the sputtering source rather than with micrometeoroid bombardment. When Phobos is in the solar wind (phase angles larger than 172.6° and lower than 10°), sputtering is a dominant source of material ejection. The stoichiometry of species in the surface is roughly conserved in the ejecta cloud. This is due to our assumption that the sputtering yields being scaled with that of Iron (i.e., sputtering is stoichiometric), whereas for the regolith's of Mercury and the Moon the most volatile species, such as Sodium, would be primarily desorbed but can return to the surface and be recycled. The average ejecta densities in the disk indeed are: $7.15 \times 10^{-2} \text{ cm}^{-3}$ for Oxygen (dashed line), $7.17 \times 10^{-2} \text{ cm}^{-3}$ for Iron (line with disks), $3.32 \times 10^{-2} \text{ cm}^{-3}$ for Magnesium (plain line), then $1.2 \times 10^{-3} \text{ cm}^{-3}$ for Aluminium (line with crosses), $2.0 \times 10^{-4} \text{ cm}^{-3}$ for Sodium (line with squares) and calcium (line with diamonds). While crossing the plasma cavity (phase angles between 46.7° and 130°), the dominant ejection process becomes micrometeoroid bombardment competing with a flux of planetary protons impacting the surface (density close to 1 cm^{-3}), leading in both cases to low degassing rates. In this region, the proton flux at Phobos' surface (not shown) quickly decreases by 4 orders of magnitude (from about 3×10^7 to $10^4 \text{ cm}^{-2} \text{ s}^{-1}$). An increase of the degassing by a factor of 2 is observed in the shocked region and the magnetosheath (see for instance between 130° and 172°), where the proton density becomes higher than in the SW

Table 2
Ejection rates of material due to micrometeoroid bombardment.

Element	Ejection rate (s^{-1})	Average ejecta speed (km s^{-1})
Fe	3.04×10^{16}	0.94
O	1.17×10^{17}	1.76
Mg	2.58×10^{16}	1.44
Al	2.89×10^{15}	1.36
Ca	2.89×10^{14}	1.11
Na	4.55×10^{14}	1.47

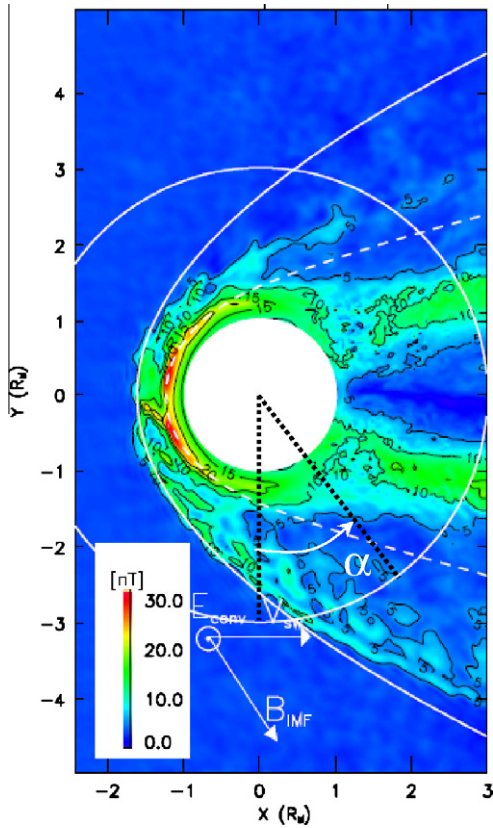


Fig. 1. Sketch of Phobos' orbit in Mars equatorial (X - Y) plane showing the phase angle α , and drawn over a distribution of the magnetic field intensity derived by Modolo et al. (2005) with an angle between the solar wind velocity vector V_{sw} and B_{IMF} of 56° . The X axis is along the Sun-Mars direction. The phase angle origin is when Phobos is on the dusk side of Mars (Y axis < 0).

region by a factor of ~ 5 . We note that heavy planetary ions (not taken into account in the present study), such as O^+ , O_2^+ and CO_2^+ , formed from neutrals escaping the planet and then convected by the electric field (e.g. Kallio et al., 2008) may also increase the sputtering rate while Phobos' orbit crosses the magnetosheath region.

The sputtering source is very sensitive to binding energies (energies needed to remove atoms/molecules from the surface) of species in Phobos' regolith, which are basically not well constrained by laboratory data. In the present study we use values ranging from 0.27 eV for Na up to 0.64 eV for Fe, which may differ significantly from actual binding energies of atomic species in minerals but are consistent with energies derived from measurements of energy distributions of sputtered elements from mineral matrices (see e.g. Wiens et al. (1997)). Therefore density values derived from our simulations have to be considered with caution. We carried out a sensitivity test of ejecta rates with respect to this parameter in the case of Mg, leading to density variations plotted in Fig. 3. The binding energy of Mg is assumed to be equal to 0.23 eV in the case of Fig. 1. For the sensitivity test, the binding energy has been varied between 0.1 and 2 eV. Ejecta densities are seen to vary by about 40% of the average values show in Fig. 3 (plain line) in this range. Such variations, that we consider as representative over the different ejected elements species, do not imply drastic changes on the composition of the ejecta cloud previously discussed.

In Fig. 4 we have plotted the spatial distribution of the main species: Fe (right column), O (middle column) and Mg (left column) present in the neutral cloud. The X axis is along the Sun-Mars axis (the Sun towards $X > 0$). The structure of the cloud is mainly constrained by the gravitational influence of Mars combined with the effect of radiation pressure. However, in our case radiation pressure forces are derived for an average position of Mars around the Sun, so that there are no seasonal effects similar to that observed on the dust torus by Krivov and Hamilton (1997). A disk structure of the ejecta cloud can be defined from density variations of the ejecta in the equatorial plane and in the

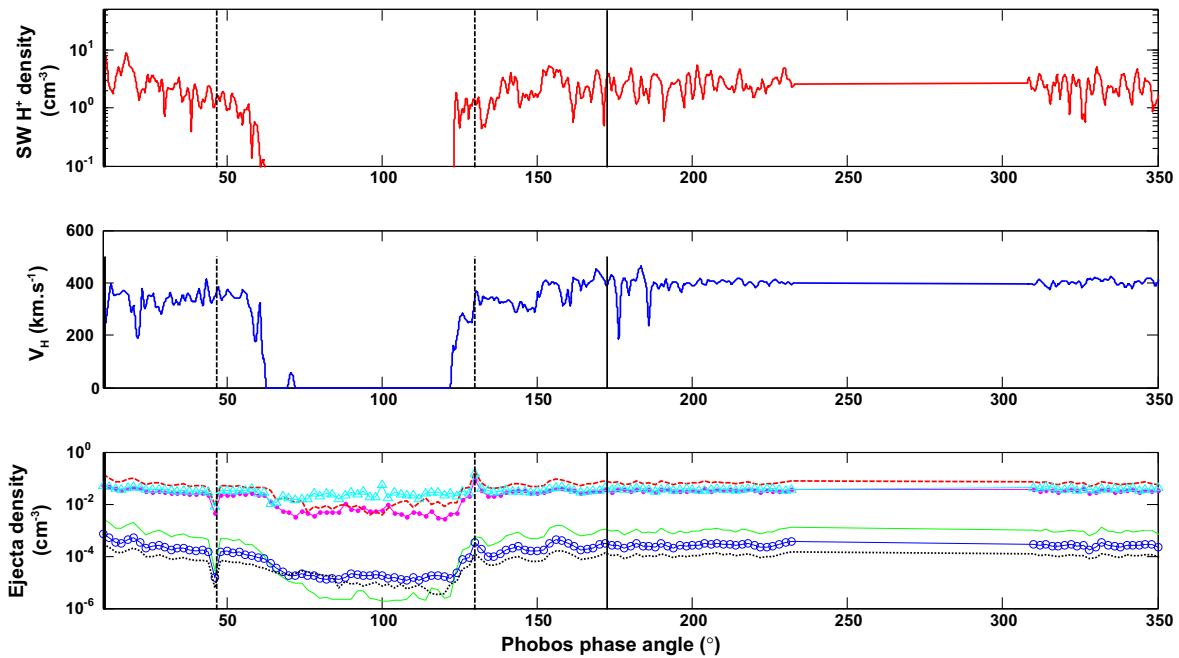


Fig. 2. Upper panel: solar wind protons density at Phobos' orbit. Middle panel: solar wind protons velocity component along the Sun-Mars axis. Lower panel: Evolution of average ejecta densities within 500 km from Phobos' surface as a function of Phobos' phase angle. Light blue line with triangles: Iron, red dashed line: Oxygen, magenta dash-dotted line: Magnesium, green solid line: Aluminium, blue line with circles: Sodium and black dotted line: Calcium. Black vertical lines (10° and 172.6°) indicate the average position of the Bow Shock in the hybrid simulation of Modolo et al. (2005), while black dashed lines (46.7° and 130°) indicate the average position of the Magnetic Piles-up Boundary crossed by Phobos.

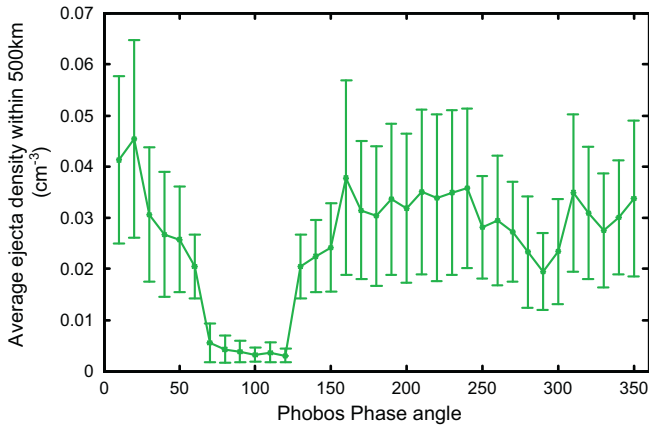


Fig. 3. Average density variations of Magnesium within 500 km of Phobos surface. Errorbars show the standard deviation of the density due to variation of the binding energy in the range (0.1–2 eV).

perpendicular plane, which are shown in Fig. 5 in the case of Mg. The disk morphology does not vary significantly between species. A ten fold decrease of the density appears within about 6 martian radii along the Sun–Mars axis (panels (a)–(c) of Fig. 4), and within over 3 martian radii in the perpendicular plane (mostly panels (d)–(f) of Fig. 4). This ejecta disk is not centered on Mars, but slightly shifted northward and towards the anti-sunward side in the case of Phobos at the subsolar point. The one order less dense cloud

when Phobos is inside the magnetotail (panels (g)–(i)) results from a weakening of the weathering process in the plasma cavity on the nightside of Mars. Such a large difference implies that the Phobos cloud should be observed preferentially when it is in the solar wind and that significant variations of in the cloud density a expected during Phobos' orbit and with respect to the solar activity.

3.2. Emission brightness

For each species we have computed line-of-sight column densities N (cm^{-2}) as seen from the Earth. In order to estimate solar scattering emission intensities as a function of Phobos' phase angle we have calculated photon scattering efficiencies (or g -factors in s^{-1}) using a high resolution solar flux model at solar minimum activity (Lemaire et al., 2005; VanHoosier et al., 1988; Kurucz et al., 1984) and absorption oscillator strengths given in Morton (2003, 2004). Emission intensities are given in units of Rayleigh by $(4\pi) \times I = 10^{-6} \times N \times g$ where the g -factor is in s^{-1} . Their values for the brightest emission lines are given in Table 3. Emissions intensities generally remain very weak, that is, except in the case of Mg, well below $10^{-1} R$. After (Bertaux et al., 2006; Leblanc et al., 2006) UV spectrometers as MEX/SPICAM around Mars could typically detect 1 R/nm at the Magnesium emission line which has a brightness of $\sim 1.4 \times 10^{-3} R/\text{nm}$, requiring unrealistic integration times. In practice emissions lower than $10^2 R$ are difficult to observe with MEX/SPICAM. In comparison, state of the art space based UV spectrograph as HST/STIS using an echelle grating would

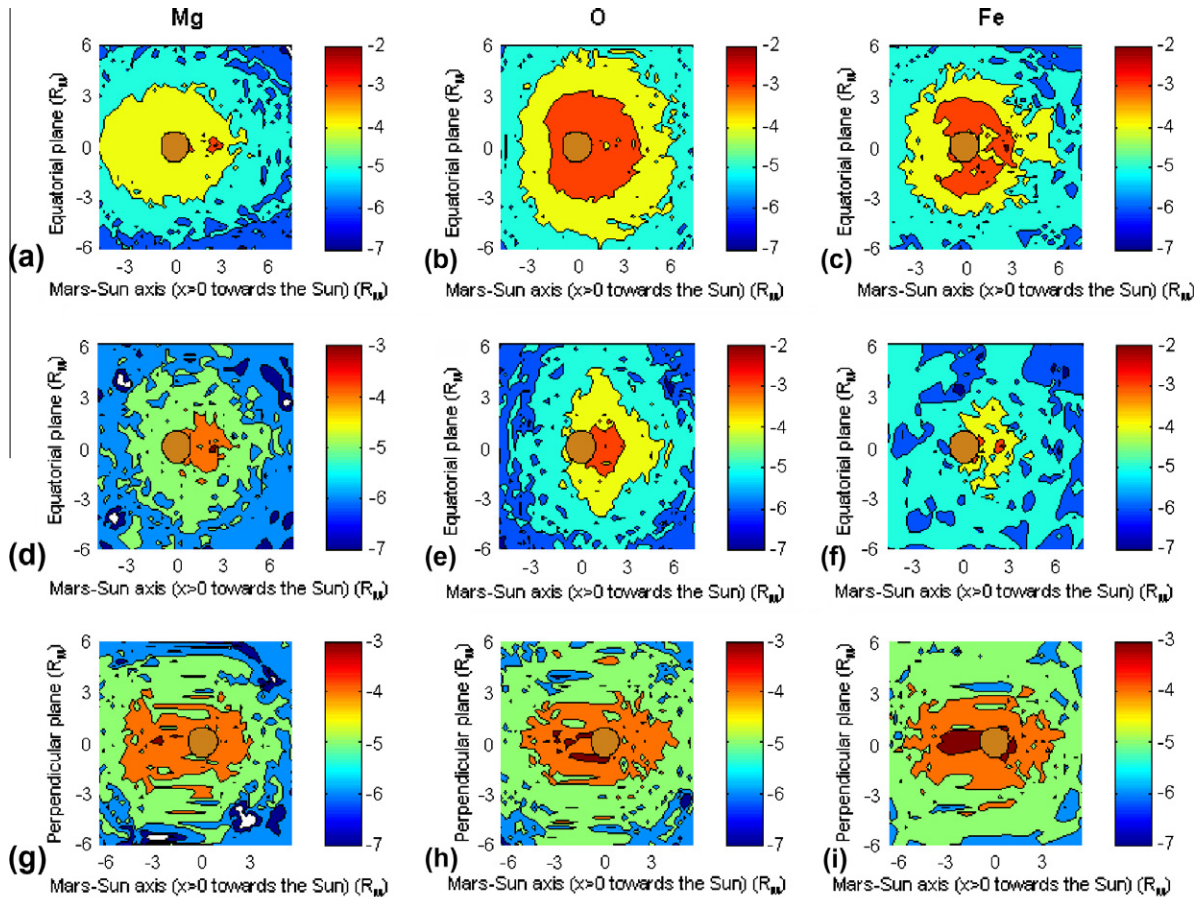


Fig. 4. Morphology of Phobos' ejecta disk for Mg, Fe, and O centered on Mars (distances are given in martian radius), in the equatorial plane (panels (a)–(c)), and in a plane perpendicular (panels (d)–(i)). The Z is oriented towards the North pole of Mars, while the X axis is aligned with the Mars–Sun direction. In panels (a)–(f), Phobos is at the subsolar point ($X = 2 R_M$, $Y = 0 R_M$), whereas its position is anti-solar in panels (g)–(i) ($X = -2 R_M$, $Y = 0 R_M$). The colorscale on the right of each panel gives the ejecta density in cm^{-3} (LOG SCALE).

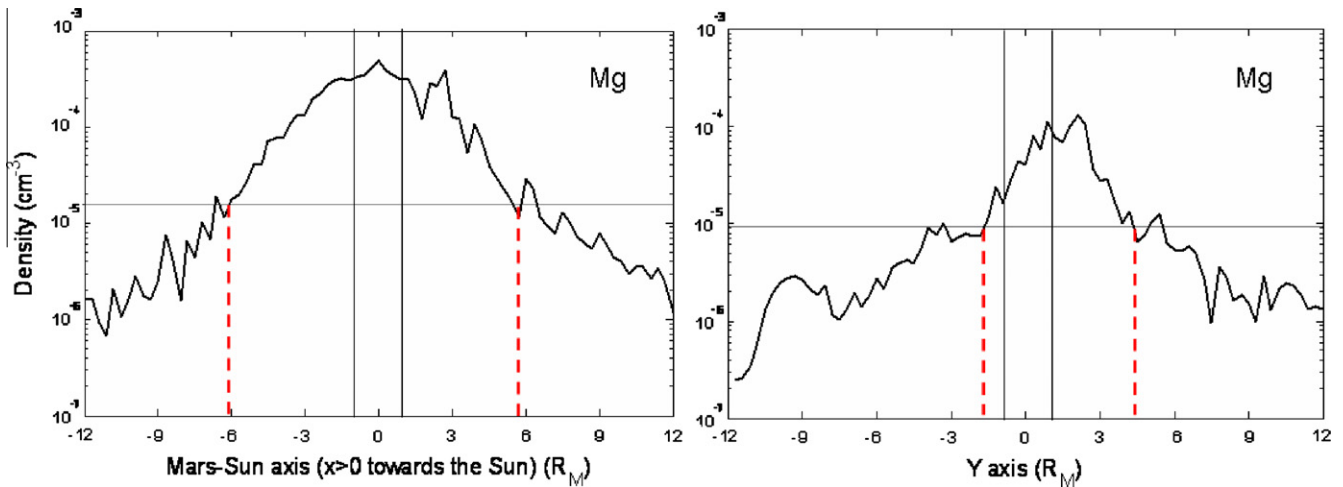


Fig. 5. Density of Magnesium along the Mars–Sun axis (left panel) and along a perpendicular axis (right panel). The disk extension (as defined in the text) along both directions is indicated by the red dashed lines. (For interpretation of the references to color in this figure legend, the reader is referred to the web version of this article.)

Table 3

Variabilities of solar scattering emission brightness in the vicinity of Phobos along Phobos orbit. Values for Fe and O are not shown because typically lower than $10^{-5} R$.

Element	Wavelength (Å)	Min (R)	Max (R)	Avg (R)	g-factor (s^{-1})
Ca	4226.728	2.1×10^{-3}	2.7×10^{-2}	1.2×10^{-2}	0.66
Na	5895.924	1.5×10^{-3}	1.0×10^{-1}	7.3×10^{-3}	0.54
Al	3944.006	8.7×10^{-4}	9.5×10^{-3}	4.4×10^{-3}	4.25×10^{-2}
Mg	2852.9631	1.2	2.1	1.5	0.41

have a limit sensitivity of $\sim 4 \times 10^{-3} R$ at 2852.9631 Å with $S/N = 10$ and 1 h integration time and $R \sim 30,000$ resolution, indicating that Magnesium may be detectable in the UV range depending on observing conditions. However, intensity values we shown here can be taken as lower limits since calculations are carried out at solar minimum conditions. Since the solar UV flux varies by up to a factor 2 from solar minimum to solar maximum, we can expect that emissions to be slightly higher at solar maximum. Moreover, Solar Energetic Particles Events may actually drive large increase of the ejection rate from the surface and therefore of the emission brightness. Therefore, observations of the Phobos cloud are likely under such conditions.

4. Discussion and conclusion

Assuming an Iron-rich composition of Phobos' surface, we carried out 3D Monte Simulation of space weathering due to both sputtering by solar wind H^+ and He^{2+} ions, and micrometeoroid bombardment, for solar minimum conditions. Following such assumptions, and assuming the principal ejecta are atomic and not molecular, the main neutral species populating the cloud is Iron, Oxygen, and Magnesium with typical densities between 10^{-2} and 10^{-3} cm^{-3} . We note that for non reactive incident ions, a significant fraction of Oxygen would be released as O_2 . However, for protons, some atoms could recombine and be released as H_2O , a process also discussed at the Moon. The sputtering source is seen to globally dominate the weathering process along Phobos' orbit, except on the nightside of Mars where planetary protons and micrometeoroid bombardments are similar. The ejecta cloud morphology is basically driven by Mars' gravitation and radiation pressure forces. By calculating the solar scattering emission intensities for the brightest lines of each species, we derive a lower limit of a

few Rayleigh in the case of Magnesium. Based on the present simulations, and keeping in mind large uncertainties associated with the calculated emission brightness values, Magnesium would therefore be the only species potentially detectable from space based telescopes or sufficiently sensitive space based UV spectrometers.

Acknowledgments

The authors would like to acknowledge two anonymous reviewers, especially one of them, for an in-depth and critical reading of the manuscript, as well as many constructive comments leading to a large improvement of the initial paper. We also acknowledge Pierre Vernazza's work on the spectral properties and composition of Phobos, providing the necessary inputs for the present study.

References

- Behrisch, R., 1980. Dependence of light-ion sputtering yields of iron on ion fluence and oxygen partial pressure. *J. Nucl. Mater.* 93–94 (Part 2), 645–655.
- Bertaux, J.L., Korabiev, O., Perrier, S., Quémerais, E., Montmessin, F., Leblanc, F., Lebonnois, S., Rannou, P., Lefèvre, F., Forget, F., Fedorova, A., Dimarellis, E., Reberac, A., Fonteyn, D., Chaufray, J.Y., Guibert, S., 2006. SPICAM on Mars Express: Observing modes and overview of UV spectrometer data and scientific results. *J. Geophys. Res.* 111, E10S90. doi:10.1029/2006JE002690.
- Bruno, M., Cremonese, G., Marchi, S., 2007. Neutral sodium atoms release from the surfaces of the Moon and Mercury induced by meteoroid impacts. *Planet. Space Sci.* 55, 1494–1501.
- Busch, M.W. et al., 2007. Arecibo radar observations of Phobos and Deimos. *Icarus* 186, 581–584.
- Christou, A.A., Beurle, K., 1999. Meteoroid streams at Mars: possibilities and implications. *Planet. Space Sci.* 47 (12), 1475–1485.
- Cintala, M.J., 1992. Impact-induced effects in the lunar and mercurian regoliths. *J. Geophys. Res.* 97, 947–973.
- Cipriani, F., Leblanc, F., Witasse, O., Johnson, R.E., 2008. Sodium recycling at Europa: What do we learn from the sodium cloud variability? *Geophys. Res. Lett.* 35, L19201.
- Cipriani, F., Leblanc, F., Witasse, O., Johnson, R.E., 2009. Exospheric signatures of alkali abundances in Europa's regolith. *Geophys. Res. Lett.* 36, L12202.
- Domokos, A., Bell III, J.F., Brown, P., Lemmon, M.T., Suggs, R., Vaubaillon, J., Cooke, W., 2007. Measurement of the meteoroid flux at Mars. *Icarus* 191, 141–150.
- Dubinin, E.M., Lundin, R., Pissarenko, N.F., Barabash, S.V., Zakharov, A.V., Koskinen, H., Schwingshuh, K., Yeroshenko, Ye.G., 1990. Indirect evidences for a gas/dust torus along the Phobos orbit. *Geophys. Res. Lett.* 17, 861–864.
- Eichhorn, G., 1978. Heating and vaporization during hypervelocity particle impact. *Planet. Space Sci.* 26, 463–467.
- Fulle, M., Leblanc, F., Harrison, R.A., Davis, C.J., Eyles, C.J., Halain, J.P., Howard, R.A., Bockelée-Morvan, D., Cremonese, G., Scarmato, T., 2007. Discovery of the atomic iron tail of Comet McNaught using the heliospheric imager on STEREO. *ApJ* 661, L93.

- Hapke, B., 2001. Space weathering from Mercury to the asteroid belt. *J. Geophys. Res.* 106, 10039–10073. doi:10.1029/2000JE001338.
- Huebner, W.F., Keady, J.J., Lyon, S.P., 1992. Solar photo rates for planetary atmospheres and atmospheric pollutants. *Astrophys. Space Sci.* 195, 1–289. 291–294.
- Ip, W.H., Banaszekiewicz, M., 1990. On the dust/gas tori of Phobos and Deimos. *Geophys. Res. Lett.* 17, 857–860.
- Jacobson, R.A., 2008. The orbits of the Martian satellites. AAS/Division for Planetary Sciences Meeting Abstracts: Vol. 40.05, pp. 46.
- Johnson, R.E., Baragiola, R., 1991. Lunar surface: Sputtering and secondary ion mass spectrometry. *Geophys. Res. Lett.* 18, 2169–2172.
- Kallio, E., Fedorov, A., Budnik, E., Barabash, S., Jarvinen, R., Janhunen, P., 2008. On the properties of O⁺ and O₂⁺ ions in a hybrid model and in Mars Express IMA/ASPERA-3 data: A case study. *Planet. Space Sci.* 56, 1204–1213.
- Killen, R.M., Potter, A.E., Reiff, P., Sarantos, M., Jackson, B.V., Hick, P., Giles, B., 2001. Evidence for space weather at Mercury. *J. Geophys. Res.* 106, 20509–20525. doi:10.1029/2000JE001401.
- Krivov, A.V., Hamilton, D.P., 1997. Martian dust belts: Waiting for discovery. *Icarus* 128, 335–353.
- Kuback, C., Sidis, V., 1981. Theoretical study of near-resonant charge exchange collisions of H⁺ with alkali atoms. *Phys. Rev. A* 23, 110–118.
- Leblanc, F., Johnson, R.E., 2003. Mercury's sodium exosphere. *Icarus* 164, 261–281.
- Kurucz, R.L., Furenlid, I., Brault, J., Testerman, L., 1984. Solar Flux Atlas from 296 to 1300 nm. National Solar Observatory Atlas, No. 1 (Sunspot: NSO).
- Leblanc, F., Potter, A.E., Killen, R.M., Johnson, R.E., 2005. Origins of Europa Na cloud and torus. *Icarus* 178 (2), 367–385.
- Leblanc, F., Chaufray, J.Y., Lilensten, J., Witasse, O., Bertaux, J.-L., 2006. Martian dayglow as seen by the SPICAM UV spectrograph on Mars Express. *J. Geophys. Res.* 111, E09S11.
- Matsuda, Y., Yamaguchi, K., Suenaga, K., Yamagata, Y., Honda, C., Maeda, M., Yamamura, Y., Muraoka, K., Akazaki, M., 1988. Measurement of preferential sputtering of iron-oxides using laser fluorescence spectroscopy. *Jpn. J. Appl. Phys.* 27, L2022–L2024.
- Morton, D.C., 2003. Atomic data for resonance absorption lines. III. Wavelengths longward of the Lyman limit for the elements hydrogen to gallium. *Astrophys. J. Suppl.* 149 (1), 149–205.
- Morton, D.C., 2004. Erratum: "Atomic data for resonance absorption lines. III. Wavelengths longward of the Lyman limit for the elements hydrogen to gallium". *Astrophys. J. Suppl.* 151 (2), 151–403.
- Modolo, R., Chanteur, G.M., Dubinin, E., Matthews, A.P., 2005. Influence of the solar EUV flux on the martian plasma environment. *Ann. Geophys.* 23, 433–444. doi:10.5194/angeo-23-433-2005.
- Molina-Cuberos, G.J., Witasse, O., Lebreton, J.P., Rodrigo, R., López-Moreno, J.J., 2003. Meteoritic ions in the atmosphere of Mars. *Planet. Space Sci.* 51, 239–249.
- Lemaire, P., Emerich, C., Vial, J.C., Curdt, W., Schühle, U., Wilhelm, K., 2005. Variation of the full Sun hydrogen Lyman profiles through solar cycle 23. *Adv. Space Res.* 35, 384–387.
- Øieroset, M., Brain, D.A., Simpson, E., Mitchell, D.L., Phan, T.D., Halekas, J.S., Lin, R.P., Acuña, M.H., Mario, H., 2010. Search for Phobos and Deimos dust tori using in situ observations from Mars Global Surveyor MAG/ER. *Icarus* 206 (1), 189–198.
- Pandey, M.K., Dubey, R.K., Tripathi, D.N., 2007. Charge exchange collisions of H⁺/D⁺ ions with alkaline Earth atoms. *Eur. Phys. J. D41*, 275–279.
- Rivkin, A.S., Brown, R.H., Trilling, D.E., Bell, J.F., Plassmann, J.H., 2002. Near-infrared spectrophotometry of Phobos and Deimos. *Icarus* 156, 64–75.
- Rutherford, J.A., Vroom, D.A., 1972. Formation of iron ions by charge transfer. *J. Chem. Phys.* 57, 3091–3093.
- Showalter, M.R., Hamilton, D.P., Douglas, P., Nicholson, P.D., 2006. A deep search of martian dust rings and inner moons using the Hubble Space Telescope. *Planet. Space Sci.* 54, 844–854.
- Soter, S., 1971. The Dust Belt of Mars. Center for Radiophysics and space Research. Cornell University, CRSR 462.
- Stebbing, R.F., Smith, A.C.H., Ehrhardt, H., 1964. Charge transfer between oxygen atoms and O⁺ and H⁺ ions. *J. Geophys. Res.* 69 (18), 2349–2355.
- Vanhoosier, Michael E., Bartoe, John-David F., Brueckner, Guenter E., Prinz, Dianne K., 1988. Absolute solar spectral irradiance 120–400 nm (results from the Solar Ultraviolet Spectral Irradiance Monitor – SUSIM – Experiment on board Spacelab 2). *Astron. Phys. Lett. Commun.* 27, 164–168.
- Vernazza, P. et al., 2010. Meteorite analogs for Phobos and Deimos: Unraveling the origin of the martian moons. In: 73rd Annual Meeting of the Meteoritical Society. Abstract #5076.
- Wiens, R.C., Burnett, D.S., Calaway, W.F., Hansen, C.S., Lykke, K.R., Pellin, M.J., 1997. Sputtering products of sodium sulfate: Implications for Io's surface and for sodium-bearing molecules in the Io torus. *Icarus* 128 (2), 386–397.